

Proposal to directly observe the Kondo effect through enhanced photo-induced scattering of cold fermionic and bosonic atoms

Bhuvanesh Sundar and Erich J. Mueller

Laboratory of Atomic and Solid State Physics, Cornell University, Ithaca NY 14850

(Dated: February 18, 2019)

We propose an experimental protocol to directly observe the Kondo effect by scattering ultracold atoms with spin-dependent interactions. We propose using an optical Feshbach resonance to engineer Kondo-type spin-dependent interactions in a system with ultracold ${}^6\text{Li}$ and ${}^{87}\text{Rb}$ gases. We calculate the momentum transferred from the ${}^{87}\text{Rb}$ to the ${}^6\text{Li}$ gas in a scattering experiment and show that it has a logarithmically enhanced temperature dependence, characteristic of the Kondo effect and analogous to the resistivity of alloys with magnetic impurities. Experimentally detecting this enhancement will give a different perspective on the Kondo effect, and allow us to explore a rich variety of problems such as the Kondo lattice problem and heavy-fermion systems.

PACS numbers: 67.85.Pq, 72.10.Fk, 72.15.Qm

I. INTRODUCTION

Ultracold atomic gases are model systems for understanding phenomena from condensed matter physics. One such intriguing phenomenon is the Kondo effect [1, 2]. In this paper we propose an experimental protocol to directly observe the scattering physics underlying the Kondo effect. Such an experiment would give a new perspective on an iconic problem.

The Kondo effect is a transport anomaly that arises when itinerant electrons interact with magnetic impurities. The source of the phenomenon is a many body bound state formed between the Fermi sea and an impurity. This bound state leads to resonant scattering of itinerant electrons off the impurities. As the temperature is lowered, this resonant scattering dominates over other scattering processes and leads to a characteristic logarithmic temperature dependence of the resistivity of the material. Despite intense research, some questions about the Kondo effect remain unresolved and some of the key theoretical predictions have never been directly seen. For example, the electron cloud which screens the spin on the impurity has never directly been imaged [3–6]. More importantly the analogous problem with an array of interacting impurities (the Kondo lattice) is not well understood [7]. Exploring the Kondo lattice problem is of paramount importance to the understanding of heavy fermion systems and quantum criticality [8, 9].

In this paper we propose using cold atoms to directly observe enhanced Kondo scattering. We envision a system consisting of a Fermi gas and a dilute Bose gas, where bosonic atoms play the role of magnetic impurities and fermionic atoms play the role of electrons. To strengthen the analogy with immobile spin impurities in the Kondo model, we consider bosons which are much heavier than the fermions. In particular we consider fermionic ${}^6\text{Li}$ and bosonic ${}^{87}\text{Rb}$, for which the recoil of the ${}^{87}\text{Rb}$ atoms can be ignored. Other bosonic atoms, such as ${}^{133}\text{Cs}$ could also be considered, leading to an even greater mass ratio. To observe the Kondo effect, we need spin-dependent collisions to dominate over spin-independent ones. We

argue that optical Feshbach resonances can be used to tune the scattering in different spin channels to reach this limit. We model this photo-enhancement of spin-dependent scattering, and find that it is large enough to enable observation of the Kondo effect at experimentally accessible temperatures.

As the temperature is lowered, one expects the Kondo effect to increase the cross-section for Bose-Fermi scattering [1]. We propose directly measuring this enhancement by launching the ${}^{87}\text{Rb}$ gas into the ${}^6\text{Li}$ gas with a small velocity. One would then measure the momentum transferred to the ${}^6\text{Li}$ atoms. A number of related experiments have been used to probe atomic scattering in the past [10–13]. We show that the final momentum of the Fermi gas varies logarithmically with temperature, analogous to the resistance of electrons in an alloy with magnetic impurities. The temperature dependence of the transferred momentum, depicted in Fig. 1, has a minimum which is a signature of the Kondo effect, and this minimum can be detected experimentally.

This paper is organized as follows. In Sec. II we introduce the Kondo model in the context of our atomic system. In Sec. III we explain how optical Feshbach resonances can be used to implement the interactions in this model. In Sec. IV we calculate the momentum exchanged in a scattering experiment between atomic clouds. We calculate this momentum transfer as a function of temperature perturbatively up to third order in the interaction strength. We take a pedagogical approach, explicitly describing all parts of our calculation. We summarize in Sec. V.

II. THE KONDO MODEL

In this section we describe the Kondo model. In the next section we describe how to engineer atomic interactions to simulate the Kondo model.

We build our system out of ${}^6\text{Li}$ and ${}^{87}\text{Rb}$ atoms in their ground state at zero magnetic field, namely the $F = 1/2$ and $F = 1$ hyperfine states. We let the operators $\hat{a}_{r\alpha}^\dagger$

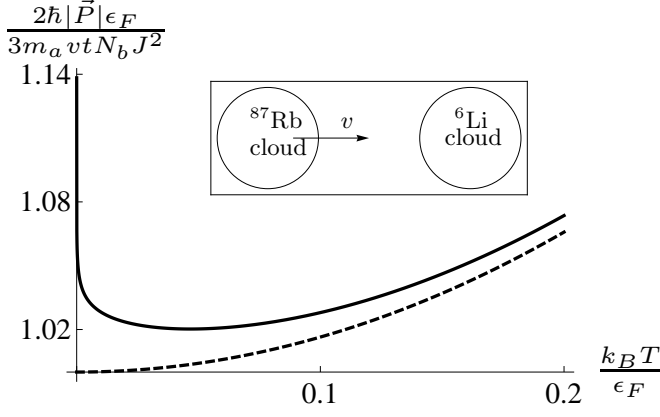


FIG. 1: Temperature dependence of the momentum \vec{P} transferred from bosons to fermions in a scattering experiment with photo-induced interactions. Solid line: Kondo-type interactions, dashed line: density-density interactions. The minimum in \vec{P} is a signature of the Kondo effect, and may be detected experimentally. Both \vec{P} and temperature have been rescaled to dimensionless quantities. The symbols ϵ_F , m_a , v , t , N_b and J denote the Fermi energy, fermion mass, launching speed of bosons, elapsed time, number of bosons, and the effective exchange coupling for spin-dependent interactions. We denote the exchange coupling for density-density interactions by J' . Here we use $J = J' = 0.01\epsilon_F$. We argue in Sec. IV that these value of J and J' are experimentally feasible. Inset shows a cartoon of the collision.

and $\hat{b}_{r\mu}^\dagger$ create ${}^6\text{Li}$ and ${}^{87}\text{Rb}$ atoms at position \vec{r} and spin projection $\alpha = \uparrow, \downarrow$ or $\mu = 0, \pm 1$ along the z-axis. Their Fourier transforms,

$$\begin{aligned} \hat{a}_{k\alpha}^\dagger &= \frac{1}{\sqrt{V}} \int d^3\vec{r} \hat{a}_{r\alpha}^\dagger e^{i\vec{k}\cdot\vec{r}}, \\ \hat{b}_{k\mu}^\dagger &= \frac{1}{\sqrt{V}} \int d^3\vec{r} \hat{b}_{r\mu}^\dagger e^{i\vec{k}\cdot\vec{r}}, \end{aligned} \quad (1)$$

create particles in momentum eigenstates. Above, V is the volume of the system.

We wish to explore a model with a Hamiltonian $\hat{H} = \hat{H}_0 + \hat{H}_{\text{int}}$, where \hat{H}_0 models the kinetic energy of the fermions and bosons,

$$\begin{aligned} \hat{H}_0 &= \frac{V}{(2\pi)^3} \int d^3\vec{k} \left(\sum_\alpha (\epsilon_k - \mu) \hat{a}_{k\alpha}^\dagger \hat{a}_{k\alpha} + \sum_\mu E_k \hat{b}_{k\mu}^\dagger \hat{b}_{k\mu} \right), \\ \epsilon_k &= \frac{\hbar^2 k^2}{2m_a}, \quad E_k = \frac{\hbar^2 k^2}{2M_b}, \end{aligned} \quad (2)$$

and \hat{H}_{int} models the interaction between them,

$$\hat{H}_{\text{int}} = g \int d^3\vec{r} \sum_{\alpha\beta\mu\nu} \hat{a}_{r\alpha}^\dagger \hat{a}_{r\beta} \hat{b}_{r\mu}^\dagger \hat{b}_{r\nu} \vec{\sigma}_{\alpha\beta}^{(a)} \cdot \vec{\sigma}_{\mu\nu}^{(b)}. \quad (3)$$

We denote the vector of spin matrices for the fermions and bosons by $\vec{\sigma}^{(a)}$ and $\vec{\sigma}^{(b)}$. It is important to note that \hat{H}_{int} contains terms where $\alpha \neq \beta$ and $\mu \neq \nu$. This is because the atoms exchange spin when they collide. It is useful to rewrite \hat{H}_{int} in momentum space as

$$\begin{aligned} \hat{H}_{\text{int}} &= g \frac{V^2}{(2\pi)^9} \int d^3\vec{k} \int d^3\vec{p} \int d^3\vec{q} \sum_{\alpha\beta\mu\nu} \hat{a}_{k+q,\alpha}^\dagger \hat{a}_{k+p,\beta} \hat{b}_{k-q,\mu}^\dagger \hat{b}_{k-p,\nu} \vec{\sigma}_{\alpha\beta}^{(a)} \cdot \vec{\sigma}_{\mu\nu}^{(b)}. \end{aligned} \quad (4)$$

The interaction in Eq. (4) is very similar to the one in the spin-1 Kondo model [1], with one exception; the ${}^{87}\text{Rb}$ atoms, which play the role of impurities, are mobile. Due to their large mass however, the recoil of the ${}^{87}\text{Rb}$ atoms can be neglected, and formally the physics is equivalent to that of immobile spin impurities.

The dominant interaction in typical cold atom experiments has a density-density form, rather than the spin-dependent form of Eq.(4). In the following, we describe how to make spin-dependent interactions dominate.

III. PHYSICAL SETUP AND EFFECTIVE MODEL

In this section we describe our proposal to experimentally achieve the Hamiltonian introduced in Sec. II. The ${}^6\text{Li}$ and ${}^{87}\text{Rb}$ atoms have quantum numbers $S = 1/2$, $L = 0$ and $I = 1$ and $3/2$. We show that optical Feshbach resonances can be used to implement controllable spin-dependent scattering.

In an optical Feshbach resonance, lasers provide a coupling between the open scattering channel and a closed channel containing a bound state [14, 15]; here the bound state is a highly excited LiRb molecular state. The electronic spins in the molecule are entangled, giving a mechanism for spin-exchange. While this optically induced spin-exchange has not yet been experimentally observed, there have been extensive studies of both elastic and inelastic scattering properties near optical Feshbach resonances [16–22]. Thus the transition frequencies for forming LiRb molecules are well known.

To independently control the spin-independent and spin-dependent scattering cross-sections, we propose coupling the atoms with two different highly excited LiRb molecular states: one with electronic spin $S = 0$ and the other with $S = 1$. Adiabatically eliminating the molecular states leads to an effective Hamiltonian between the atoms that is parameterized by exactly two parameters. By tuning the frequencies of the lasers in our setup, we set the interaction to be of the form of Eq.(3). Below we provide a mathematical framework to model the optical Feshbach resonances and show how to choose the parameters. All the physics described in this section is local, and we have dropped the index labeling the position of the atoms from the second-quantized operators.

The energy density for the relevant electronic and nuclear degrees of freedom in each atom and molecule is of the form

$$\hat{H} = \hat{H}_{\text{HF}}^{\text{Li}} + \hat{H}_{\text{HF}}^{\text{Rb}} + \hat{H}_{\text{Fesh}}^{(S=0)} + \hat{H}_{\text{Fesh}}^{(S=1)} + \hat{H}_{\text{mol}}. \quad (5)$$

\hat{H}_{mol} describes the binding energies of the molecules:

$$\begin{aligned} \hat{H}_{\text{mol}} &= \sum_{mm'} E_b \hat{\gamma}_{mm'}^{(S=0)\dagger} \hat{\gamma}_{mm'}^{(S=0)} \\ &+ \sum_{msmm'} E_b' \hat{\gamma}_{mm'}^{(S=1,ms)\dagger} \hat{\gamma}_{mm'}^{(S=1,ms)}, \end{aligned} \quad (6)$$

where $\hat{\gamma}_{mm'}^{(S)\dagger}$ creates a molecule with a spin S , and E_b and E'_b are their binding energies. The indices m and m' label the nuclear spins of the ${}^6\text{Li}$ and ${}^{87}\text{Rb}$ atoms.

The hyperfine Hamiltonians for the atoms are

$$\begin{aligned}\hat{H}_{\text{HF}}^{\text{Li}} &= hA_{\text{Li}} \sum_{\substack{m_S, m'_S \\ m_I, m'_I}} \hat{a}_{m_S m_I}^\dagger \hat{a}_{m'_S m'_I} \vec{\sigma}_{m_S m'_S}^{(1/2)} \cdot \vec{\sigma}_{m_I m'_I}^{(1)} \\ \hat{H}_{\text{HF}}^{\text{Rb}} &= hA_{\text{Rb}} \sum_{\substack{m_S, m'_S \\ m_I, m'_I}} \hat{b}_{m_S m_I}^\dagger \hat{b}_{m'_S m'_I} \vec{\sigma}_{m_S m'_S}^{(1/2)} \cdot \vec{\sigma}_{m_I m'_I}^{(3/2)}\end{aligned}\quad (7)$$

where h is Planck's constant, $A_{\text{Li}} = 152\text{MHz}$ and $A_{\text{Rb}} = 3.4\text{GHz}$ are the hyperfine coupling constants of ${}^6\text{Li}$ and ${}^{87}\text{Rb}$ [23], $\vec{\sigma}^{(S)}$ is the vector of spin- S matrices, and $\hat{a}_{m_S m_I}^\dagger$ and $\hat{b}_{m_S m_I}^\dagger$ create a ${}^6\text{Li}$ and ${}^{87}\text{Rb}$ atom in the state $|m_S m_I\rangle$. In terms of the hyperfine eigenstates,

$$|m_S, m_I\rangle = \sum_{F, m_F} C_{m_S m_I}^{F m_F} |F, m_F\rangle \quad (8)$$

where $C_{m_S m_I}^{F m_F}$ are Clebsch-Gordan coefficients.

The terms in $\hat{H}_{\text{Fesh}}^{(S=0)}$ and $\hat{H}_{\text{Fesh}}^{(S=1)}$ describe the interactions between the photo-association lasers and the atoms, respectively coupling to spin-0 and spin-1 molecules. We first consider the coupling to spin-0 molecules, such as those labeled by ${}^1\Sigma_+$ or ${}^1\Pi$. We model this photo-induced molecular formation by

$$\hat{H}_{\text{Fesh}}^{(S=0)} = \sum_{mm'} \Omega e^{i(\vec{k}\cdot\vec{r}-\omega t)} \hat{\gamma}_{mm'}^{(S=0)\dagger} \frac{\hat{a}_{\frac{1}{2}m} \hat{b}_{-\frac{1}{2}m'} - \hat{a}_{-\frac{1}{2}m} \hat{b}_{\frac{1}{2}m'}}{\sqrt{2}} + \text{h.c.} \quad (9)$$

where \vec{r} is the position of the atoms, and $\hbar\vec{k}$ and ω are the momentum and frequency of the laser photon inducing molecule formation. The detuning between the atomic and molecular states is $\hbar\omega - E_b$.

Another laser forms spin-1 molecules such as those labeled by ${}^3\Sigma_+$ or ${}^3\Pi$. We model this process by

$$\begin{aligned}\hat{H}_{\text{Fesh}}^{(S=1)} &= \sum_{mm'} \Omega' e^{i(\vec{k}'\cdot\vec{r}-\omega't)} \\ &\times \left(\hat{\gamma}_{mm'}^{(S=1, m_S=1)\dagger} \hat{a}_{\frac{1}{2}m} \hat{b}_{\frac{1}{2}m'} + \hat{\gamma}_{mm'}^{(S=1, m_S=0)\dagger} \frac{\hat{a}_{\frac{1}{2}m} \hat{b}_{-\frac{1}{2}m'} - \hat{a}_{-\frac{1}{2}m} \hat{b}_{\frac{1}{2}m'}}{\sqrt{2}} + \hat{\gamma}_{mm'}^{(S=1, m_S=-1)\dagger} \hat{a}_{-\frac{1}{2}m} \hat{b}_{-\frac{1}{2}m'} \right) + \text{h.c.}\end{aligned}\quad (10)$$

where $\hbar\vec{k}'$ and ω' are the momentum and frequency of the laser photon.

When $E_b - \hbar\omega \gg \Omega$ and $E'_b - \hbar\omega' \gg \Omega'$, the occupation in the molecular states will be small. Therefore we can

adiabatically eliminate the molecular states and obtain an effective interaction between the ${}^6\text{Li}$ and ${}^{87}\text{Rb}$ atoms using second order perturbation theory:

$$\begin{aligned}\hat{H}_{\text{int}} &= \sum_{mm'} \frac{\Omega^2}{E_b - \hbar\omega} \left(\frac{\hat{a}_{\frac{1}{2}m} \hat{b}_{-\frac{1}{2}m'} - \hat{a}_{-\frac{1}{2}m} \hat{b}_{\frac{1}{2}m'}}{\sqrt{2}} \right)^\dagger \left(\frac{\hat{a}_{\frac{1}{2}m} \hat{b}_{-\frac{1}{2}m'} - \hat{a}_{-\frac{1}{2}m} \hat{b}_{\frac{1}{2}m'}}{\sqrt{2}} \right) \\ &+ \frac{\Omega'^2}{E'_b - \hbar\omega'} \left(\hat{a}_{\frac{1}{2}m} \hat{b}_{\frac{1}{2}m'}^\dagger \hat{a}_{\frac{1}{2}m} \hat{b}_{\frac{1}{2}m'} + \left(\frac{\hat{a}_{\frac{1}{2}m} \hat{b}_{-\frac{1}{2}m'} + \hat{a}_{-\frac{1}{2}m} \hat{b}_{\frac{1}{2}m'}}{\sqrt{2}} \right)^\dagger \left(\frac{\hat{a}_{\frac{1}{2}m} \hat{b}_{-\frac{1}{2}m'} + \hat{a}_{-\frac{1}{2}m} \hat{b}_{\frac{1}{2}m'}}{\sqrt{2}} \right) + \hat{a}_{-\frac{1}{2}m} \hat{b}_{-\frac{1}{2}m'}^\dagger \hat{a}_{-\frac{1}{2}m} \hat{b}_{-\frac{1}{2}m'} \right).\end{aligned}\quad (11)$$

Using Eq.(8), the operators $\hat{a}_{m_S m_I}^\dagger$ and $\hat{b}_{m_S m_I}^\dagger$ can be projected into the hyperfine eigenstate basis. Assuming that the chemical potential is set such that the $F = 3/2$ and $F = 2$ manifolds are unoccupied, we project \hat{H}_{int}

into the $F = 1/2$ and $F = 1$ manifolds. We obtain an effective interaction

$$\hat{H}_{\text{int}} = \sum_{\alpha\beta\mu\nu} \hat{a}_\alpha^\dagger \hat{a}_\beta \hat{b}_\mu^\dagger \hat{b}_\nu \left(\frac{1}{6} \vec{\sigma}_{\alpha\beta}^{(a)} \cdot \vec{\sigma}_{\mu\nu}^{(b)} \left(\frac{\Omega^2}{E_b - \hbar\omega} - \frac{\Omega'^2}{E'_b - \hbar\omega'} \right) + \frac{1}{4} \delta_{\alpha\beta} \delta_{\mu\nu} \left(\frac{\Omega^2}{E_b - \hbar\omega} + 3 \frac{\Omega'^2}{E'_b - \hbar\omega'} \right) \right). \quad (12)$$

The first term in Eq.(12) is of the form of Kondo-like interactions in Eq.(3), and the second term a density-density interaction. By tuning $\frac{\Omega^2}{E_b - \hbar\omega}$ to equal $-3\frac{\Omega'^2}{E'_b - \hbar\omega'}$, we can engineer \hat{H}_{int} to equal \hat{H}_{int} . Any background density-density interactions can be eliminated by further adjusting these parameters. To explore Kondo physics, $g = \frac{1}{6} \left(\frac{\Omega^2}{E_b - \hbar\omega} - \frac{\Omega'^2}{E'_b - \hbar\omega'} \right)$ should be positive. Researchers implementing optical Feshbach resonances with alkali atoms typically use frequencies such that $\hbar\omega - E_b$ and $\hbar\omega' - E'_b$ are on the order of $\hbar \times 100\text{MHz}$, and produce $\Omega^2, \Omega'^2 \sim 10^{-2}\hbar^2\text{cm}^3/\text{s}^2$ using laser intensities of $\sim 50\text{W}/\text{cm}^2$ (for example, see [16, 17]). As a result, they achieve interaction strengths $g \sim 10^{-10}\hbar\text{cm}^3/\text{s}$, where g was defined in Eq.(3). At a fermion density of $n \sim 10^{14}\text{cm}^{-3}$, this yields $gn \sim 0.01\epsilon_F$. For comparison, the background ^6Li - ^{87}Rb scattering has $g_{\text{bg}} \sim 10^{-11}\hbar\text{cm}^3/\text{s}$.

IV. KONDO-ENHANCED SCATTERING BETWEEN ^{87}Rb AND ^6Li

Through the Kondo effect, the interaction engineered in Sec. III will lead to an enhanced cross-section for Bose-Fermi scattering at low temperatures. In this section we propose an experiment to directly observe this enhancement and calculate its temperature dependence.

We imagine launching the ^{87}Rb gas into the ^6Li gas with a small velocity \vec{v} . The duration of interaction between an ^{87}Rb atom and the ^6Li gas is $t = L/v$ where L is the size of the ^6Li cloud. We calculate the momentum transferred from the ^{87}Rb gas to the ^6Li gas at time t to zeroth order in $1/M_b$, first order in \vec{v} and third order in the interaction parameter g . Since L is a macroscopic quantity and we work in the small v limit, we make a long time approximation wherever possible. We assume that the ^{87}Rb atoms are dilute, and neglect events involving scattering of a ^6Li atom with more than one ^{87}Rb atom. Equivalently, we calculate the momentum transferred by one ^{87}Rb atom with momentum $M_b\vec{v}$, and sum over all ^{87}Rb atoms. The Fermi surface of ^6Li will play an important role. We find a logarithmic temperature dependence of the transferred momentum, characteristic of the Kondo effect, and analogous to the behavior of electrical resistance of magnetic alloys. As shown in Fig. 1, this leads to a minimum in the momentum transferred.

We consider the collision of the Fermi gas with one ^{87}Rb atom with spin projection m at time 0. The momentum of the Fermi gas at time t is then $\vec{P}_m = \frac{V}{(2\pi)^3} \int d^3\vec{k} \sum_{\alpha} \hbar\vec{k} n_{k\alpha m}(t)$, where

$$n_{k\alpha m}(t) = \langle \hat{b}_{M_b v, m}(0) \hat{a}_{k\alpha}^{\dagger}(t) \hat{a}_{k\alpha}(t) \hat{b}_{M_b v, m}^{\dagger}(0) \rangle \quad (13)$$

is the occupation of fermions with momentum \vec{k} and spin projection α at time t . In Eq.(13), $\hat{a}_{k\alpha}(t)$ is a Heisenberg operator and the expectation value is taken over a thermal ensemble of fermions, with no bosons

present. Since the ^{87}Rb atoms are spin-unpolarized, the average momentum imparted by a ^{87}Rb atom is $\vec{P}_{av} = \frac{V}{3(2\pi)^3} \int d^3\vec{k} \sum_{\alpha m} \hbar\vec{k} n_{k\alpha m}(t)$. Multiplying by N_b , the number of bosons, the net momentum of the Fermi gas is

$$\vec{P}(t) = \frac{N_b V}{3(2\pi)^3} \int d^3\vec{k} \sum_{\alpha m} \hbar\vec{k} n_{k\alpha m}(t). \quad (14)$$

A. Diagrammatic expansion

The standard way to calculate quantities like $n_{k\alpha m}(t)$ in Eq.(13) is using the S-matrix [24]:

$$n_{k\alpha m}(t) = \langle T \hat{S} \hat{b}_{M_b v, m}(0) \hat{a}_{k\alpha}^{\dagger}(t) \hat{a}_{k\alpha}(t) \hat{b}_{M_b v, m}^{\dagger}(0) \rangle_0, \quad (15)$$

$$\hat{S} = e^{-i \int d\tau \hat{H}_{\text{int}}(\tau)},$$

where T orders the operators along a path shown in Fig. 2 which starts at time 0, passes through time t , and returns to time 0. All our integrals over time follow this path. The notation $\langle \rangle_0$ implies that all operators inside $\langle \rangle_0$ evolve according to

$$\begin{aligned} \hat{a}_{k\alpha}(t) &= e^{i\hat{H}_0 t/\hbar} \hat{a}_{k\alpha} e^{-i\hat{H}_0 t/\hbar}, \\ \hat{b}_{k\mu}(t) &= e^{i\hat{H}_0 t/\hbar} \hat{b}_{k\mu} e^{-i\hat{H}_0 t/\hbar}, \end{aligned} \quad (16)$$

and states are weighted by $e^{-\beta\hat{H}_0}$. Since \hat{H}_0 is quadratic in $\hat{a}_{k\alpha}$ and $\hat{b}_{k\mu}$, the right hand side of $n_{k\alpha m}(t)$ in Eq.(15) can be contracted using Wick's theorem. As a result, $n_{k\alpha m}(t)$ can be expressed diagrammatically as a sum of Feynman's diagrams. We calculate these Feynman's diagrams up to $O(g^3)$.

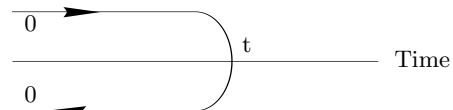


FIG. 2: In our integrals, time begins at 0, passes through t , then returns to 0. Our perturbation theory requires ordering operators along this path.

B. Feynman rules

We denote the propagator for fermions, $\langle T \hat{a}_{k\alpha}(t_1) \hat{a}_{k\alpha}^{\dagger}(t_2) \rangle_0$, by a solid line, and the propagator for bosons, $\langle T \hat{b}_{k\mu}(t_1) \hat{b}_{k\mu}^{\dagger}(t_2) \rangle_0$, by a dotted line, depicted in Figs. 3(a) and 3(b). Their values are

$$\begin{aligned} \langle T \hat{a}_{k\alpha}(t_1) \hat{a}_{k\alpha}^{\dagger}(t_2) \rangle_0 &= e^{-i\epsilon_k(t_1 - t_2)} (\Theta(t_1 - t_2) - f_k), \\ \langle T \hat{b}_{k\mu}(t_1) \hat{b}_{k\mu}^{\dagger}(t_2) \rangle_0 &= e^{-iE_k(t_1 - t_2)} \Theta(t_1 - t_2), \end{aligned} \quad (17)$$

where $f_k = \frac{1}{e^{\beta(\epsilon_k - \mu)} + 1}$ is the Fermi occupation factor. In Eq.(17), $\Theta(t_1 - t_2) = 1$ if t_1 is after t_2 along the path in Fig. 2, and 0 otherwise.

We perturbatively expand $n_{k\alpha m}(t)$ in the vertex depicted in Fig. 3(c), whose value is

$$\begin{array}{c} \begin{array}{c} \text{---} \nearrow \\ \text{---} \searrow \\ \text{---} \nwarrow \\ \text{---} \swarrow \end{array} \\ \begin{array}{c} k_4, \mu \\ k_2, \alpha \end{array} \end{array} \begin{array}{c} \text{---} \nwarrow \\ \text{---} \swarrow \\ \text{---} \nearrow \\ \text{---} \searrow \end{array} \begin{array}{c} k_3, \nu \\ k_1, \beta \end{array} = \frac{(2\pi)^3 g}{V^2} \vec{\sigma}_{\alpha\beta}^{(1/2)} \cdot \vec{\sigma}_{\mu\nu}^{(1)} \delta(k_1 + k_3 - k_2 - k_4). \end{array} \quad (18)$$

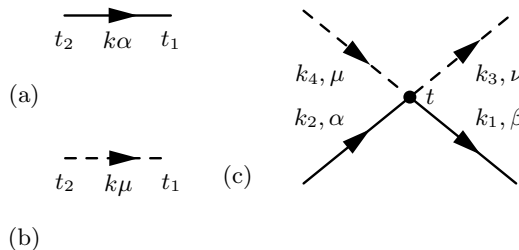


FIG. 3: Diagrammatic representation of vertex and propagators. a) Solid line denotes a fermion propagator which propagates a fermion with momentum k and spin projection α from time t_2 to t_1 . b) Dashed line denotes a boson propagator which propagates a boson with momentum k and spin projection μ from time t_2 to t_1 . c) A vertex denotes the matrix element for a Bose-Fermi scattering event. Mathematical expressions are given in Eqs.(17) and (18).

The vertex denotes a scattering event between a fermion and a boson. The time at which this scattering event occurs is integrated over the path in Fig. 2. All momenta and spin projections are summed/integrated over, with the constraint that momenta and spin are conserved at each vertex. The diagrams which contribute to Eq.(14) have four external propagators. There is an incoming and outgoing fermion propagator evaluated at time t , and carrying momentum $\hbar\vec{k}$ and spin projection α . There is also an incoming and outgoing boson propagator evaluated at time 0, and carrying momentum $M_b\vec{v}$ and spin projection m . All lines and vertices in a Feynman diagram can be labeled using the rules described above. Therefore we omit labels. Finally, each diagram carries a multiplicity, which is the number of times it appears in the expansion of Eq.(15) in powers of g .

C. Calculation of $n_{k\alpha m}(t)$

In this section we calculate Eq.(15). Terms of $O(g^n)$ in the expansion contain $2n+2$ pairs of operators leading to $(n+1)!^2$ contractions. The resulting number of diagrams increases exponentially with n . We explicitly consider each order and evaluate the non-zero diagrams. The first non-zero contribution comes at second order, where our expansion reproduces Fermi's golden rule. At third order, we find the Kondo enhancement which gives rise to

a logarithmic temperature dependence of \vec{P} (defined in Eq.(14)) at small temperatures and long times.

1. Zeroth order

The zeroth order process does not involve any Bose-Fermi scattering. The expression for the zeroth order term in the expansion of $n_{k\alpha m}(t)$ is

$$n_{k\alpha m}^{(0)}(t) = \langle T \hat{b}_{M_b v, m}(0) \hat{a}_{k\alpha}^\dagger(t) \hat{a}_{k\alpha}(t) \hat{b}_{M_b v, m}^\dagger(0) \rangle_0. \quad (19)$$

Using Wick's theorem,

$$\begin{aligned} n_{k\alpha m}^{(0)}(t) &= \langle \hat{b}_{M_b v, m}(0) \hat{b}_{M_b v, m}^\dagger(0) \rangle_0 \langle \hat{a}_{k\alpha}^\dagger(t) \hat{a}_{k\alpha}(t) \rangle_0 \\ &= f_k. \end{aligned} \quad (20)$$

The corresponding Feynman diagram is shown in Fig. 4. Since the bosons and fermions do not interact at this order, $n_{k\alpha m}^{(0)}$ does not contribute to any momentum transfer.

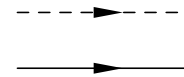


FIG. 4: Zeroth order diagram in the expansion for $n_{k\alpha m}(t)$.

2. First order

The first order term in the expansion for $n_{k\alpha m}(t)$ is

$$\begin{aligned} n_{k\alpha m}^{(1)}(t) &= -i \int d\tau_1 \\ &\langle T \hat{H}_{\text{int}}(\tau_1) \hat{b}_{M_b v, m}(0) \hat{a}_{k\alpha}^\dagger(t) \hat{a}_{k\alpha}(t) \hat{b}_{M_b v, m}^\dagger(0) \rangle_0. \end{aligned} \quad (21)$$

By Wick-contracting the above expression, we find that

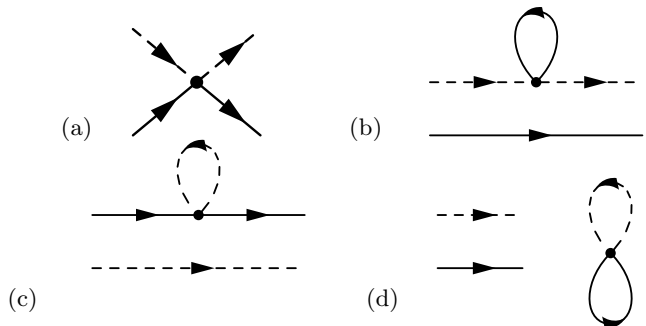


FIG. 5: First order diagrams in the expansion of $n_{k\alpha m}(t)$.

$n_{k\alpha m}^{(1)}(t)$ is the sum of the four diagrams shown in Fig. 5. Of these Figs. 5(b), (c) and (d) are zero. For example the vertex in Fig. 5(b) is proportional to the azimuthal spin of the fermion in the fermion loop. Therefore the term where the loop fermion has azimuthal spin 1/2 cancels the term where the loop fermion has azimuthal spin

$-1/2$. The diagrams in Figs. 5(c) and 5(d) can also be shown to be zero based on similar reasoning. Moreover, the same reasoning implies that all higher order diagrams in which a fermion or boson loop begins and ends at the same vertex are also zero.

The Feynman rule for a vertex (in Eq.(18)) implies that the diagram in Fig. 5(a) is proportional to the spin projection m of the bosons. Since the ^{87}Rb atoms are spin-unpolarized, the average momentum imparted by a ^{87}Rb atom at this order is zero. Therefore, for any k and α ,

$$\frac{1}{3} \sum_m n_{k\alpha m}^{(1)}(t) = 0. \quad (22)$$

The absence of a first order contribution is not surprising, as we know that the cross-section is at least quadratic in the coupling between ^6Li and ^{87}Rb .

3. Second order

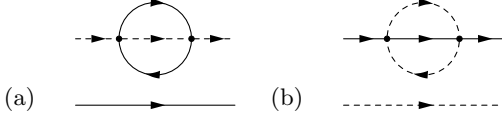


FIG. 6: Two of the diagrams that are zero at second order.

The second order term,

$$n_{k\alpha m}^{(2)}(t) = -\frac{1}{2} \int d\tau_1 d\tau_2 \langle T \hat{H}_{\text{int}}(\tau_1) \hat{H}_{\text{int}}(\tau_2) \hat{b}_{M_b v, m}(0) \hat{a}_{k\alpha}^\dagger(t) \hat{a}_{k\alpha}(t) \hat{b}_{M_b v, m}^\dagger(0) \rangle_0, \quad (23)$$

can be contracted into Wick pairs in 36 ways, which give rise to 20 different diagrams. Most of these diagrams are zero because of reasons explained in Sec. IV C 2. In addition, the diagrams shown in Fig. 6 also evaluate to zero. For example, since we work in the dilute boson limit, there can only be one boson line in any time slice, resulting that Fig. 6(a) is zero. The only two non-zero diagrams are shown in Fig. 7.

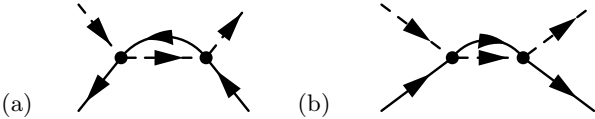


FIG. 7: Non-zero diagrams at $O(g^2)$ in the expansion for $n_{k\alpha m}(t)$.

Using our Feynman rules,

$$\frac{1}{3} \sum_m \text{diagram} = \frac{2g^2}{V(2\pi)^3} \int d^3\vec{p} (1-f_k) f_p \frac{\sin^2 \delta\epsilon t/\hbar}{\delta\epsilon^2} \quad (24)$$

and

$$\frac{1}{3} \sum_m \text{diagram} = -\frac{2g^2}{V(2\pi)^3} \int d^3\vec{p} f_k (1-f_p) \frac{\sin^2 \delta\epsilon' t/\hbar}{\delta\epsilon'^2}, \quad (25)$$

where $\delta\epsilon = \frac{1}{2} \left(\epsilon_k - \epsilon_p - \frac{1}{2} M_b v^2 + \frac{(\hbar\vec{k} - \hbar\vec{p} - M_b \vec{v})^2}{2M_b} \right)$ and $\delta\epsilon' = \frac{1}{2} \left(\epsilon_k - \epsilon_p + \frac{1}{2} M_b v^2 - \frac{(\hbar\vec{k} - \hbar\vec{p} + M_b \vec{v})^2}{2M_b} \right)$. Neglecting terms of order $1/M_b$, $\delta\epsilon = \delta\epsilon' = \frac{1}{2} (\epsilon_k - \epsilon_p)$. The resulting second order contribution is

$$\frac{1}{3} \sum_m n_{k\alpha m}^{(2)}(t) = -\frac{g^2}{V(2\pi)^3} \int d^3\vec{p} (f_k - f_p) \frac{\sin^2 t\delta\epsilon/\hbar}{\delta\epsilon^2}. \quad (26)$$

Since the bosons are much heavier than the fermions, they have nearly the same velocity \vec{v} before and after scattering. Therefore, it is easier to work in the bosons' rest frame. For small \vec{v} ,

$$\begin{aligned} \frac{1}{3} \sum_m n_{k+\frac{m\vec{a}v}{\hbar}, \alpha m}^{(2)}(t) &= -\frac{g^2}{V(2\pi)^3} \int d^3\vec{p} \left(f_k - f_p + \hbar\vec{k} \cdot \vec{v} \frac{\partial f_k}{\partial \epsilon_k} - \hbar\vec{p} \cdot \vec{v} \frac{\partial f_p}{\partial \epsilon_p} \right) \\ &\times \frac{\sin^2(t(\epsilon_k - \epsilon_p)/2\hbar)}{((\epsilon_k - \epsilon_p)/2)^2} + O(v^2, 1/M_b). \end{aligned} \quad (27)$$

The notation $O(v^2, 1/M_b)$ denotes that we have neglected terms which scale as v^2 or $1/M_b$. The first two terms in Eq.(27) have negligible contribution near $\epsilon_k = \epsilon_p$. At long times, any significant contribution due to them comes from the tail of $\frac{\sin^2(t(\epsilon_k - \epsilon_p)/2\hbar)}{((\epsilon_k - \epsilon_p)/2)^2}$, where $\sin^2(t(\epsilon_k - \epsilon_p)/2\hbar)$ can be approximated by its average, $1/2$. Hence their contribution saturates to a constant at long times. For the last two terms (in Eq.(27)) which are significant near $\epsilon_k = \epsilon_p$, we approximate $\frac{\sin^2(t(\epsilon_k - \epsilon_p)/2\hbar)}{((\epsilon_k - \epsilon_p)/2)^2} \simeq \frac{2t\delta(\epsilon_k - \epsilon_p)}{\hbar}$. Hence at long times,

$$\begin{aligned} \frac{1}{3} \sum_m n_{k+\frac{m\vec{a}v}{\hbar}, \alpha m}^{(2)}(t) &= -\frac{2g^2 t}{V(2\pi)^3} \int d^3\vec{p} \left(\vec{k} \cdot \vec{v} \frac{\partial f_k}{\partial \epsilon_k} - \vec{p} \cdot \vec{v} \frac{\partial f_p}{\partial \epsilon_p} \right) \delta(\epsilon_k - \epsilon_p) \\ &+ O\left(t^0, v^2, \frac{1}{M_b}\right) \\ &= -2 \left(\frac{g}{V}\right)^2 t \vec{k} \cdot \vec{v} \frac{\partial f_k}{\partial \epsilon_k} \rho(\epsilon_k) + O\left(t^0, v^2, \frac{1}{M_b}\right), \end{aligned} \quad (28)$$

where $\rho(\epsilon_k)$ is the 3D density of states for a single spin projection. In the lab frame,

$$\frac{1}{3} \sum_m n_{k\alpha m}^{(2)}(t) = -2 \left(\frac{g}{V}\right)^2 t \vec{k} \cdot \vec{v} \frac{\partial f_k}{\partial \epsilon_k} \rho(\epsilon_k) + O\left(t^0, v^2, \frac{1}{M_b}\right). \quad (29)$$

Equation (29) is the result one obtains from Fermi's golden rule. One obtains the same expression for the case where the fermions and bosons have a density-density interaction as well. Kondo physics is apparent only in third order.

4. Third order

The third order term

$$n_{k\alpha m}^{(3)}(t) = \frac{i}{6} \int d\tau_1 d\tau_2 d\tau_3 (T \hat{H}_{\text{int}}(\tau_1) \hat{H}_{\text{int}}(\tau_2) \hat{H}_{\text{int}}(\tau_3) \hat{b}_{M_b v, m}(0) \hat{a}_{k\alpha}^\dagger(t) \hat{a}_{k\alpha}(t) \hat{b}_{M_b v, m}^\dagger(0))_0 \quad (30)$$

$$\frac{1}{3} \sum_m n_{k\alpha m}^{(3)}(t) = \frac{g^3}{2V(2\pi)^6} \int d^3\vec{p} \int d^3\vec{q} \frac{(2f_p-1)(f_k-f_q)}{\epsilon_{k-m_a v/\hbar} - \epsilon_{p-m_a v/\hbar}} \frac{\sin(t(\epsilon_{k-m_a v/\hbar} - \epsilon_{q-m_a v/\hbar})/2\hbar)}{(\epsilon_{k-m_a v/\hbar} - \epsilon_{q-m_a v/\hbar})/2} \frac{\sin(t(\epsilon_{p-m_a v/\hbar} - \epsilon_{q-m_a v/\hbar})/2\hbar)}{(\epsilon_{p-m_a v/\hbar} - \epsilon_{q-m_a v/\hbar})/2} + O(1/M_b). \quad (31)$$

After a treatment similar to the one at second order, Eq.(31) simplifies to

$$\frac{1}{3} \sum_m n_{k\alpha m}^{(3)}(t) = \frac{g^3}{V(2\pi)^6} \int d^3\vec{p} \, t \vec{v} \cdot \vec{k} \rho(\epsilon_k) \frac{\partial f_k}{\partial \epsilon_k} \frac{2f_p-1}{\epsilon_k - \epsilon_p} + O\left(t^0, v^2, \frac{1}{M_b}\right). \quad (32)$$

The right hand side of Eq.(32) consists of an ultraviolet divergent term arising from $\int d^3\vec{p} \frac{1}{\epsilon_k - \epsilon_p}$, and a finite term $\int d^3\vec{p} \frac{f_p}{\epsilon_k - \epsilon_p}$ which will ultimately give rise to a logarithmic temperature dependence. The ultraviolet divergence is an artefact of choosing a contact potential between the fermions and bosons which is non-zero only when they are at the same location in space. In reality, the interaction between the fermions and bosons has a finite range, which removes the ultraviolet divergence by introducing an upper cutoff on the limits on the integral over momenta. The exact details are unimportant if we express our results in terms of physical quantities. To that end, the terms involving $\int d^3\vec{p} \frac{1}{\epsilon_k - \epsilon_p}$ renormalize the interaction parameter g to an effective coupling g_{eff} given by

$$g_{\text{eff}}^2 = g^2 + \frac{g^3}{2(2\pi)^3} \int d^3\vec{p} \frac{1}{\epsilon_k - \epsilon_p}. \quad (33)$$

g_{eff} is the experimentally measured coupling between the fermions and bosons. This renormalization of g to g_{eff} occurs at all orders of perturbation theory.

D. Final momentum of the Fermi gas

We calculated in Sec. IV C that

$$\frac{1}{3} \sum_m n_{k\alpha m}(t) = f_k - 2 \left(\frac{g_{\text{eff}}}{V}\right)^2 t \vec{k} \cdot \vec{v} \frac{\partial f_k}{\partial \epsilon_k} \rho(\epsilon_k) \times \left(1 - \frac{g_{\text{eff}}}{(2\pi)^3} \int d^3\vec{p} \frac{f_p}{\epsilon_k - \epsilon_p}\right) + O\left(t^0, v^2, \frac{1}{M_b}\right). \quad (34)$$

In this section, we calculate the final momentum of the Fermi gas at long times and low temperatures, and plot

can be contracted into Wick pairs in 576 ways. However due to reasons explained in Secs. IV C 2 and IV C 3 all diagrams except the ones shown in Fig. 8 are zero. Using the Feynman rules in Eqs. (17) and (18),

the result in Fig. 1. In our calculations, we take into account the temperature dependence of the fermionic chemical potential, $\mu = \epsilon_F \left(1 - \frac{\pi^2}{12} \left(\frac{k_B T}{\epsilon_F}\right)^2\right) + O\left(\frac{k_B T}{\epsilon_F}\right)^4$.

The total momentum \vec{P} of the Fermi gas (defined in Eq.(14)) will be along the direction of \vec{v} . Its magnitude is

$$|\vec{P}| = \frac{\vec{v} \cdot \vec{P}}{v} = -\frac{4t\hbar N_b g_{\text{eff}}^2}{vV(2\pi)^3} \int d^3\vec{k} \left(\vec{k} \cdot \vec{v}\right)^2 \frac{\partial f_k}{\partial \epsilon_k} \rho(\epsilon_k) \times \left(1 - \frac{g_{\text{eff}}}{(2\pi)^3} \int d^3\vec{p} \frac{f_p}{\epsilon_k - \epsilon_p}\right). \quad (35)$$

After integrating out the angular co-ordinates of \vec{k} and performing a change of variables,

$$|\vec{P}| = -\frac{8m_a L N_b}{3\hbar V^2} g_{\text{eff}}^2 \int d\epsilon \epsilon \frac{\partial f(\epsilon)}{\partial \epsilon} \rho^2(\epsilon) \times \left(1 - \frac{g_{\text{eff}}}{V} \int d\epsilon_p \frac{\rho(\epsilon_p) f(\epsilon_p)}{\epsilon - \epsilon_p}\right). \quad (36)$$

where $L = vt$ is the size of the ${}^6\text{Li}$ cloud. We calculate Eq.(36) in two steps. First we calculate the contribution due to terms of $O(g_{\text{eff}}^2)$, then we calculate the terms of $O(g_{\text{eff}}^3)$.

We evaluate the second order terms using a Sommerfeld expansion,

$$|\vec{P}_2| \simeq \frac{3m_a L N_b}{2\hbar \epsilon_F} J^2 \left(1 + \frac{\pi^2}{6} \left(\frac{k_B T}{\epsilon_F}\right)^2\right) + O\left(\frac{k_B T}{\epsilon_F}\right)^4 \quad (37)$$

where $J = g_{\text{eff}} \frac{N}{V}$ and $\frac{N}{V}$ is the number density of fermions. As mentioned earlier in Sec. IV C 3, one obtains the same expression at second order for scattering between fermions and bosons with only a density-density interaction.

The third order terms are

$$|\vec{P}_3| = \frac{8m_a L N_b}{3\hbar} \left(\frac{g_{\text{eff}}}{V}\right)^3 \int d\epsilon \epsilon \frac{\partial f(\epsilon)}{\partial \epsilon} \rho^2(\epsilon) \times \int d\epsilon_p \frac{\rho(\epsilon_p) f(\epsilon_p)}{\epsilon - \epsilon_p} = -\frac{9m_a L N_b}{8\hbar \epsilon_F^{9/2}} J^3 \int_0^\infty d\epsilon \epsilon^2 \frac{\partial f(\epsilon)}{\partial \epsilon} \int_0^\infty d\epsilon_p \sqrt{\epsilon_p} \frac{f(\epsilon_p)}{\epsilon - \epsilon_p}. \quad (38)$$

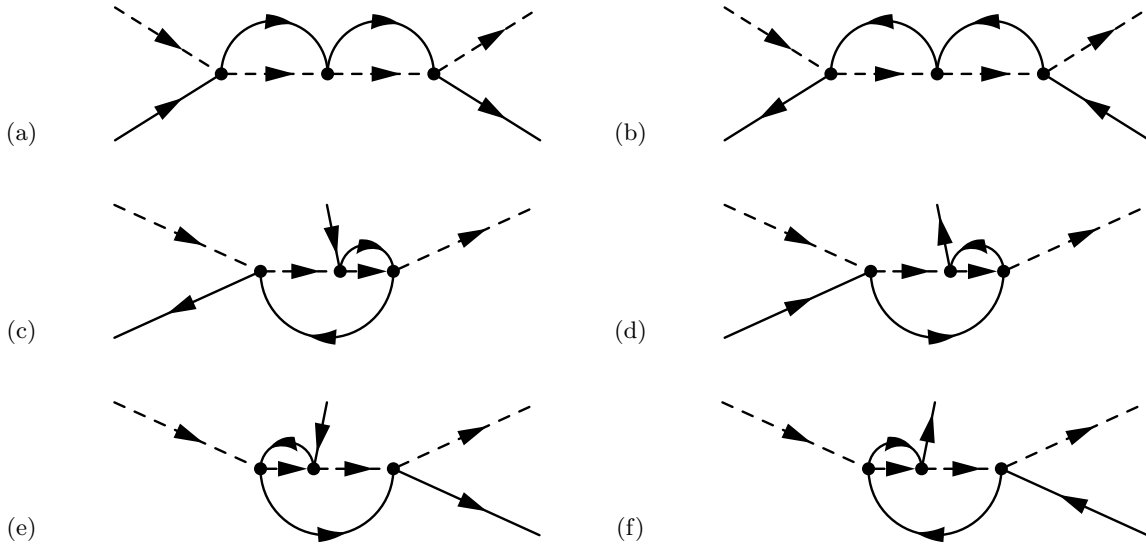


FIG. 8: Non-zero diagrams at $O(g^3)$ in the expansion for $n_{kam}(t)$.

We simplify the above expression by performing integration by parts,

$$\begin{aligned}
 |\vec{P}_3| &= \frac{9m_a L N_b}{4\hbar\epsilon_F^{9/2}} J^3 \int_0^\infty d\epsilon \epsilon^2 \frac{\partial f(\epsilon)}{\partial \epsilon} \\
 &\quad \times \int_0^\infty d\epsilon_p f(\epsilon_p) \frac{\partial}{\partial \epsilon_p} \left(\sqrt{\epsilon_p} + \frac{\sqrt{\epsilon}}{2} \log \left| \frac{\sqrt{\epsilon} - \sqrt{\epsilon_p}}{\sqrt{\epsilon} + \sqrt{\epsilon_p}} \right| \right) \\
 &= -\frac{9m_a L N_b}{4\hbar\epsilon_F^{9/2}} J^3 \int_0^\infty d\epsilon \epsilon^2 \frac{\partial f(\epsilon)}{\partial \epsilon} \\
 &\quad \times \int_0^\infty d\epsilon_p \frac{\partial f(\epsilon_p)}{\partial \epsilon_p} \left(\sqrt{\epsilon_p} + \frac{\sqrt{\epsilon}}{2} \log \left| \frac{\beta(\epsilon - \epsilon_p)}{\beta(\sqrt{\epsilon} + \sqrt{\epsilon_p})^2} \right| \right). \quad (39)
 \end{aligned}$$

We split Eq.(39) into two terms. We evaluate one of these terms numerically,

$$\begin{aligned}
 &\int_0^\infty d\epsilon \epsilon^{5/2} \frac{\partial f(\epsilon)}{\partial \epsilon} \int_0^\infty d\epsilon_p \frac{\partial f(\epsilon_p)}{\partial \epsilon_p} \log(\beta(\epsilon - \epsilon_p)) \\
 &\simeq \epsilon_F^{5/2} \left(0.26 + 5.2 \left(\frac{k_B T}{\epsilon_F} \right)^2 \right) + O\left(\frac{k_B T}{\epsilon_F} \right)^4. \quad (40)
 \end{aligned}$$

We use a Sommerfeld expansion for the remaining term. The result is

$$|\vec{P}_3| \simeq -\frac{9m_a L N_b}{4\hbar\epsilon_F^2} J^3 \left(1.13 + \left(2.6 - \frac{\pi^2}{48} \right) \left(\frac{k_B T}{\epsilon_F} \right)^2 + \frac{1}{2} \log \frac{k_B T}{4\epsilon_F} \left(1 + \frac{5\pi^2}{12} \left(\frac{k_B T}{\epsilon_F} \right)^2 \right) \right) + O\left(\frac{k_B T}{\epsilon_F} \right)^4. \quad (41)$$

The final momentum of the Fermi gas is

$$\vec{P} = \frac{3m_a \bar{v} L N_b J^2}{2\hbar\epsilon_F v} \left(1 + \frac{\pi^2}{6} \left(\frac{k_B T}{\epsilon_F} \right)^2 - \frac{3J}{2\epsilon_F} \left(1.13 + \left(2.6 - \frac{\pi^2}{48} \right) \left(\frac{k_B T}{\epsilon_F} \right)^2 + \frac{1}{2} \log \frac{k_B T}{4\epsilon_F} \left(1 + \frac{5\pi^2}{12} \left(\frac{k_B T}{\epsilon_F} \right)^2 \right) \right) \right), \quad (42)$$

where as before, we neglect terms of $O(t^0, v^2, \frac{1}{M_b}, T^4)$. This result is plotted in Fig. 1. The logarithmic temperature dependence of \vec{P} is characteristic of Kondo physics. Equation (42) is valid up to temperatures

$\frac{k_B T}{\epsilon_F} \simeq O\left(\frac{m_a}{M_b}\right)$. Below this temperature, the logarithmic increase saturates to a constant. Calculation of this saturation is the subject of the Kondo problem.

The result derived in Eq.(42) has very different low-temperature behavior from the momentum transferred to

a Fermi gas in the case of spin-independent Fermi-Bose interactions. As mentioned earlier in Sec. II, cold atom experiments typically have interactions of this form, modeled by

$$\hat{H}'_{\text{int}} = \frac{g'}{\sqrt{2}} \int d^3\vec{r} \sum_{\alpha\beta\mu\nu} \hat{a}_{r\alpha}^\dagger \hat{a}_{r\beta} \hat{b}_{r\mu}^\dagger \hat{b}_{r\nu} \vec{\sigma}_{\alpha\beta}^{(a)} \cdot \vec{\sigma}_{\mu\nu}^{(b)}. \quad (43)$$

An analogous calculation of the momentum transferred for this interaction yields

$$\vec{P}' = \vec{P}_2 = \frac{3m_a v_L N_b J'^2}{2\hbar\epsilon_F v} \left(1 + \frac{\pi^2}{6} \left(\frac{k_B T}{\epsilon_F} \right)^2 \right) + O \left(\frac{k_B T}{\epsilon_F} \right)^4, \quad (44)$$

where $J' = g'_{\text{eff}} n$, and g'_{eff} is defined similar to g_{eff} . For comparison, we plot this result also in Fig. 1. The most distinct difference between Eqs.(42) and (44) is that the Kondo-like interactions lead to a minimum in the momentum transferred at a temperature $T_{\text{min}} \sim \frac{3\sqrt{J\epsilon_F}}{2\pi k_B}$ while the spin-independent interactions do not. A typical experiment performed with a laser intensity $I \sim 50\text{W}/\text{cm}^2$ and a fermion density $n \sim 10^{14}\text{cm}^{-3}$ yields $J \sim 0.01\epsilon_F$, which results in a minimum for \vec{P} at $T_{\text{min}} \sim 0.05\epsilon_F/k_B$. The observation of this minimum will be a direct experimental confirmation of Kondo physics.

V. SUMMARY

We considered scattering between clouds of ^6Li and ^{87}Rb atoms. We proposed a method to engineer Kondo-

type spin-dependent interactions between them. We argued that these interactions would give rise to enhanced Fermi-Bose scattering. We perturbatively calculated the temperature-dependence of the momentum transferred to the ^6Li gas in a scattering experiment, up to third order in the Bose-Fermi interaction strength. We showed that the temperature dependence of the momentum transferred has a minimum and is logarithmic at low temperatures, characteristic of the Kondo effect and analogous to the behavior of electrical resistance in magnetic alloys.

The ground state of a Bose-Fermi mixture with Kondo-type spin-dependent interactions should display correlations, with each boson surrounded by a screening cloud of fermions with opposite spin. These clouds may be observable through various imaging techniques. Similar experiments with bosons confined to a lattice would probe an analog of the Kondo lattice problem. One can explore other techniques to experimentally engineer Kondo-type interactions. For example, one can realize the Anderson model and Kondo-like situations by trapping the impurities in a deep optical lattice [25].

ACKNOWLEDGEMENTS

We acknowledge support from ARO-MURI Non-equilibrium Many-body Dynamics grant (W911NF-14-1-0003).

-
- [1] J. Kondo, *Prog. Theor. Phys.* **32**, 37 (1964).
 - [2] A. C. Hewson, *The Kondo problem to heavy fermions*, 2 (Cambridge university press, 1997).
 - [3] I. Affleck, arXiv:0911.2209 (2009).
 - [4] I. Affleck, in *Strongly Correlated Fermions and Bosons in Low-Dimensional Disordered Systems* (Springer, 2002), pp. 1–12.
 - [5] J. B. Boyce and C. P. Slichter, *Phys. Rev. B* **13**, 379 (1976).
 - [6] J. B. Boyce and C. P. Slichter, *Phys. Rev. Lett.* **32**, 61 (1974).
 - [7] H. Tsunetsugu, M. Sigrist, and K. Ueda, *Rev. Mod. Phys.* **69**, 809 (1997).
 - [8] Z. Fisk, J. L. Sarrao, J. L. Smith, and J. D. Thompson, *Proc. Natl. Acad. Sci.* **92**, 6663 (1995).
 - [9] Z. Fisk, H. Ott, and G. Aeppli, *Jap. J. Appl. Phys.* **26**, 1882 (1987).
 - [10] R. A. Williams, L. J. LeBlanc, K. Jimenez-Garcia, M. C. Beeler, A. R. Perry, W. D. Phillips, and I. B. Spielman, *Science* **335**, 314 (2012).
 - [11] N. R. Thomas, N. Kjærgaard, P. S. Julienne, and A. C. Wilson, *Phys. Rev. Lett.* **93**, 173201 (2004).
 - [12] S. D. Gensemer, R. B. Martin-Wells, A. W. Bennett, and K. Gibble, *Phys. Rev. Lett.* **109**, 263201 (2012).
 - [13] N. Robins, C. Figl, J. Close, et al., *Optics express* **16**, 13893 (2008).
 - [14] P. Fedichev, Y. Kagan, G. Shlyapnikov, and J. Walraven, *Phys. Rev. Lett.* **77**, 2913 (1996).
 - [15] K. M. Jones, E. Tiesinga, P. D. Lett, and P. S. Julienne, *Rev. Mod. Phys.* **78**, 483 (2006).
 - [16] S. Dutta, J. Lorenz, A. Altaf, D. S. Elliott, and Y. P. Chen, *Phys. Rev. A* **89**, 020702 (2014).
 - [17] S. Dutta, D. S. Elliott, and Y. P. Chen, *EPL (Europhysics Letters)* **104**, 63001 (2013).
 - [18] M. Theis, G. Thalhammer, K. Winkler, M. Hellwig, G. Ruff, R. Grimm, and J. H. Denschlag, *Phys. Rev. Lett.* **93**, 123001 (2004).
 - [19] D. Wang, J. Qi, M. Stone, O. Nikolayeva, H. Wang, B. Hattaway, S. Gensemer, P. Gould, E. Eyler, and W. Stwalley, *Phys. Rev. Lett.* **93**, 243005 (2004).
 - [20] A. Grochola, A. Pashov, J. Deiglmayr, M. Repp, E. Tiemann, R. Wester, and M. Weidemüller, *J. Chem. Phys.* **131**, 054304 (2009).
 - [21] S. D. Kraft, P. Staunum, J. Lange, L. Vogel, R. Wester, and M. Weidemüller, *J. Phys. B* **39**, 19 (2006).
 - [22] V. V. Ivanov, A. Khramov, A. H. Hansen, W. H. Dowd, F. Münchow, A. O. Jamison, and S. Gupta, *Phys. Rev. Lett.* **106**, 153201 (2011).

- [23] E. Arimondo, M. Inguscio, and P. Violino, *Rev. Mod. Phys.* **49**, 31 (1977).
- [24] G. D. Mahan, *Many-particle physics* (Springer, 2000).
- [25] J. Bauer, C. Salomon, and E. Demler, *Phys. Rev. Lett.* **111**, 215304 (2013).